applied optics

Pattern-illuminated Fourier ptychography microscopy with a pattern-estimation algorithm

Ruizhi Cao,[1,†] Tingting Yang,[1,†] Yue Fang,[1] Cuifang Kuang,[1,2,*] and Xu Liu[1,2]

[1]State Key Laboratory of Modern Optical Instrumentation, College of Optical Science and Engineering, Zhejiang University, Hangzhou 310027, China
[2]Collaborative Innovation Center of Extreme Optics, Shanxi University, Taiyuan 030006, China
*Corresponding author: cfkuang@zju.edu.cn

Received 24 April 2017; revised 12 July 2017; accepted 24 July 2017; posted 24 July 2017 (Doc. ID 293259); published 17 August 2017

In this paper we proposed a new method that combines random pattern illumination, the pattern-estimation algorithm, and the Fourier ptychography (FP) algorithm to recover a super-resolution image. We shifted one multispot pattern to different positions to capture images, and estimated these illumination patterns using a gradient descent algorithm that shares the same root with blind structured illumination microscopy (SIM). Based on the captured images and estimated patterns, the FP algorithm is then applied to recover a super-resolution image. Our method, termed as pattern-estimated Fourier ptychography (PEFP) microscopy, does not need the prior information about the scanning position, and is thus insensitive to rotational errors and shift errors. The performance of PEFP has been demonstrated both in simulations and experiments, and PEFP achieves better resolution than the pattern-illuminated FP method when shift errors appear in our simulations. Moreover, PEFP shows strong resistance towards aberrations and works fine when there is noise in the captured image. Compared with a newly proposed blind-SIM method, PEFP also shows better resolution enhancement both in our simulations and experiments. Our method also provides the possibility to extend the application of pattern-illuminated FP to any illumination pattern because we estimated every illumination pattern separately, as blind-SIM does.

OCIS codes: (180.2520) Fluorescence microscopy; (100.6640) Superresolution; (100.3010) Image reconstruction techniques.

https://doi.org/10.1364/AO.56.006930

1. INTRODUCTION

Over the past few decades, various methods, such as stimulate emission depletion microscopy (STED) [1], photoactivated localization microscopy (PALM) [2], stochastic optical reconstruction microscopy (STORM) [3], and structured illumination microscopy (SIM) [4,5], were introduced to improve the resolution of optical microscopy based on fluorescent labeling samples. Among these methods, SIM was valued due to its fast imaging speed and wide field nature. Typically, in the conventional SIM, a well-defined sinusoidal illumination pattern was used to down-modulate the high spatial frequency information into the system's object transfer function (OTF) support, which expanded the effective OTF support region. With the prior knowledge of the illumination patterns, such as the period and the phase of the illumination patterns, reconstruction algorithms were proposed to synthesize the aperture, and up to 2× resolution improvement could be obtained theoretically. Various algorithms have been proposed to reconstruct the image with optimized phase obtained from the raw data [6–8].

However, the reconstruction algorithm may fail, owing to the distortion of illumination patterns caused by aberrations and experimental errors [8]. In order to mitigate this experimental difficulty, blind-SIM [9] was introduced, providing the possibility to reconstruct a high-resolution image without knowing the precise information of the illumination patterns. The only constraint of blind-SIM is that the sum of all illumination patterns should be uniform. There have been several algorithms proposed to improve the blind-SIM algorithm, like the joint support recovery method [10] and pattern-estimated structured illumination microscopy with a statistical priori and pixel reassignment (PE-SIMS-PR) [11]. However, the former method is sensitive to the parameter tuning [11], and the latter method runs into some problems when a low-intensity signal appears, as shown in our experimental result.

Multifocal structured illumination microscopy [12] provides a more robust method to deal with distortion using a multispot illumination pattern and realizes the same resolution improvement as conventional SIM does. But a pinhole and knowledge of the step position of the pattern are required in this method, which makes the system more complex than the typical setup of the conventional SIM and blind-SIM.

Similar to blind-SIM, pattern-illuminated Fourier ptychography [13,14] (piFP) reconstructs the high-resolution image via

random speckles, but this method requires knowledge of the exact scanning position of the random speckles, and shift errors will lead to distortions and a poorer resolution, as stated in Ref. [13].

In this paper, we proposed a new method that combines random pattern illumination, the pattern-estimation algorithm, and the Fourier ptychography (FP) algorithm to recover a super-resolution image. We shift one multispot pattern to different positions to capture images and estimate this illumination pattern using a gradient descent algorithm that shares the same root with blind-SIM. Based on the captured images and estimated patterns, the FP algorithm is then applied to recover a super-resolution image. Compared with piFP, pattern-estimated Fourier ptychography (PEFP), proposed in this paper, does not need the prior information about the scanning position, and is thus insensitive to rotational errors and shift errors. PEFP can recover the pattern and achieve the same theoretical resolution improvement as blind-SIM and provides a better resolution enhancement in our experiments compared with a proposed recent method that is based on blind-SIM. Moreover, PEFP shows great resistance to aberrations, as a digital aberration correction step is introduced to the reconstruction algorithm.

2. PRINCIPLES

PEFP uses the same captured images obtained under random illumination patterns to reconstruct the high-resolution image. We present the mechanism behind our theory in the following two sections. In the first section, the forward model of the imaging process under pattern illumination is proposed. In the second section, we demonstrate how PEFP reconstructs the illumination pattern and the sample image. The patterns and the sample image are updated separately. The sample image stays the same while the pattern is updated sequentially. Then, in the sample estimation algorithm, we update the sample image while the estimated illumination patterns stay the same.

A. Forward Model of the Imaging Process

The image that is acquired when the i-th illumination pattern $p_i(\vec{r})$ is projected onto the sample plane and can be written as

$$I_i(\vec{r}) = [p_i(\vec{r}) \cdot S(\vec{r})] * h_{\mathrm{de}}(\vec{r}), \tag{1}$$

where $I_i(\vec{r})$ denotes the i-th captured image, $S(\vec{r})$ denotes the fluorescence distribution, $h_{\mathrm{de}}(\vec{r})$ denotes the system's detection point spread function (PSF), and * indicates the convolution product.

Similar to the idea of blind-SIM, the minimization function in our algorithm is

$$f = \sum_{\vec{r}} [S_{\mathrm{est}}(\vec{r}) \cdot p_{i,\mathrm{est}}(\vec{r}) * h_{\mathrm{de}}(\vec{r}) - I_i(\vec{r})]^2, \tag{2}$$

where $p_{i,\mathrm{est}}(\vec{r})$ stands for the estimation of the i-th illumination pattern, and $S_{\mathrm{est}}(\vec{r})$ denotes the estimation of the sample. When there is no noise in the system, and both $S_{\mathrm{est}}(\vec{r})$ and $p_{i,\mathrm{est}}(\vec{r})$ are identical to their true value, the function f will reach a minimum value zero. Then we can estimate the illumination patterns and the sample using this prior knowledge.

B. Pattern and Sample Image Reconstruction

We first reconstruct the pattern with the sample image fixed. Using the same assumption that the sum of all illumination patterns is uniform, we can first write the initial guess of the sample as

$$S_{\mathrm{est\_initial}} = \sum_i I_i(\vec{r}). \tag{3}$$

We use the Richardson–Lucy deconvolution method to obtain a better estimation of the real fluorescence distribution $S(\vec{r})$, which is used as the fixed sample image of the pattern update algorithm. Then we will update our pattern in the following steps.

1. Pattern Reconstruction

The partial derivation of the function with respect to $p_{i,\mathrm{est}}(\vec{r})$ is

$$\frac{\partial f}{\partial p_{i,\mathrm{est}}} = 2[(S_{\mathrm{est}} \cdot p_{i,\mathrm{est}} * h_{\mathrm{de}} - I_i) * h_{\mathrm{de}}] \cdot S_{\mathrm{est}}. \tag{4}$$

As we have calculated the partial derivation of function f, we can use the derivation value to obtain an updated $p_{i,\mathrm{est}}$, which makes the function value smaller. Using a gradient descent method, the updated pattern $\tilde{p}_{i,\mathrm{est}}^{\mathrm{update}}(\vec{r})$, which starts with a zero matrix, can be written as follows:

$$\tilde{p}_{i,\mathrm{est}}^{\mathrm{update}} = p_{i,\mathrm{est}} - k\frac{\partial f}{\partial p_{i,\mathrm{est}}}, \tag{5}$$

where the positive number k is the updated step parameter. The value of the updated step k will decrease when the function value f is greater than the former value. As we know, the intensity of the illumination pattern should be non-negative, so when a negative value shows in the updated estimated pattern, we set the negative value to zero, which can be expressed as

$$\tilde{p}_{i,\mathrm{est}}^{\mathrm{update}} = G(\tilde{p}_i) = \begin{cases} \tilde{p}_i(\vec{r}), & \tilde{p}_i(\vec{r}) \geq 0 \\ 0, & \tilde{p}_i(\vec{r}) < 0 \end{cases}. \tag{6}$$

Owing to the fact that the illumination pattern that we project onto the sample also has a maximum spatial frequency equal to $\frac{\mathrm{NA}}{0.5\lambda_{\mathrm{ex}}}$ (λ_{ex} denotes the excitation wavelength), so we also set the frequency component of the updated pattern beyond the OTF support to zero by applying a low-pass filter,

$$F_{\tilde{p}_{i,\mathrm{est}}^{\mathrm{update}}} = L(\tilde{p}) = \begin{cases} F_{p_i}(\vec{k}), & |\vec{k}| < \frac{\mathrm{NA}}{0.5\lambda_{\mathrm{ex}}} \\ 0, & |\vec{k}| \geq \frac{\mathrm{NA}}{0.5\lambda_{\mathrm{ex}}} \end{cases}, \tag{7}$$

where F_{p_i} denotes the Fourier transform of p_i. This process will repeat until the mean-square-error (MSE) of the sequential updated two results reach convergence.

2. Sample Reconstruction

As we obtain an updated illumination pattern via the pattern reconstruction algorithm, we make the illumination pattern fixed and update the sample image.

The FP algorithm calculates the differential in the Fourier domain with respect to $S_{\mathrm{est}}(\vec{r})$, and the updated algorithm will be as follows, written in the same form as in Ref. [13]:

$$F_{S_{i,\mathrm{est}}^{\mathrm{update}}} = F_{S_{\mathrm{est}} \cdot p_{i,\mathrm{est}}} + (F_{I_i} - F_{S_{\mathrm{est}} \cdot p_{i,\mathrm{est}}} \cdot \mathrm{OTF}_{\mathrm{de}}) \cdot \mathrm{OTF}_{\mathrm{de}}. \tag{8}$$

The inverse Fourier transform of $F_{S_{i,\mathrm{est}}^{\mathrm{update}}}$ is then used to update the high-resolution image of the fluorescent sample:

$$S_{\text{est}}^{\text{update}} = S_{\text{est}} + \frac{p_{i,\text{est}}}{\max(p_{i,\text{est}})^2}(S_{i,\text{est}} - S_{\text{est}} \cdot p_{i,\text{est}}). \quad (9)$$

Based on the same nature of non-negative properties of the sample image, we also force the negative value appeared in $S_{\text{est}}^{\text{update}}$ to zero:

$$S_{\text{est}}^{\text{update}} = G(S_{\text{est}}^{\text{update}}) = \begin{cases} S_{\text{est}}^{\text{update}}(\vec{r}), & S_{\text{est}}^{\text{update}}(\vec{r}) \geq 0 \\ 0, & S_{\text{est}}^{\text{update}}(\vec{r}) < 0 \end{cases}. \quad (10)$$

To ameliorate the image result when aberrations appear, several digital correction methods were introduced to correct the aberration both in coherent imaging and incoherent imaging [15–17]. Here we add another step [16] to reduce the influence of the aberration. We use the theoretical detection OTF when the updating algorithm runs, and it will also be updated as the reconstruction goes:

$$\text{OTF}_{\text{de}}^{\text{update}} = \text{OTF}_{\text{de}} + \frac{|F_{S_{\text{est}} \cdot p_{i,\text{est}}}| \cdot \text{conj}(F_{S_{\text{est}} \cdot p_{i,\text{est}}}) \cdot [F_{I_i} - \text{OTF}_{\text{de}} \cdot F_{S_{\text{est}} \cdot p_{i,\text{est}}}]}{\max(|F_{S_{\text{est}} \cdot p_{i,\text{est}}}|)[|F_{S_{\text{est}} \cdot p_{i,\text{est}}}|^2 + \varepsilon]}, \quad (11)$$

where conj(·) denotes the complex conjugate, and ε is a positive regularization constant related to noise that is introduced to get rid of the zero denominator. The algorithm will also repeat until the MSE of the sequential updated images converge.

3. Iteration Method to Acquire a High-Resolution Image

As the initial guess of the sample image differs from the ground truth, and the updated $S_{\text{est}}^{\text{update}}$ stands for a better estimation of the sample fluorescent distribution, we set $S_{\text{est}} = S_{\text{est}}^{\text{update}}$ and repeat the process described in Sections 2.B.1 and 2.B.2. This progress continues until the MSE of $S_{\text{est}}^{\text{update}}$ is smaller than the predefined tolerance.

3. SIMULATION RESULTS

As we demonstrated in Section 2.A, random speckles can be used as the illumination pattern with only a statistic constraint. However, the speed of our algorithm will be slowed down using random speckle patterns compared with the multispot pattern. This is because more images are required, using random speckle patterns to obtain almost the same result as multispot patterns do in most cases. Based on the reason above, we apply multispot patterns in our simulations and experiments. Although there are arguments about whether the multispot pattern or the sinusoidal pattern is the best choice to obtain a super-resolution image, we use the multispot as our illumination pattern due to the fact that a well-defined sinusoidal pattern with a large spatial frequency is hard to achieve in our projection-based system, shown in Section 4.

We simulate the imaging process using our forward model and shift a multispot illumination pattern 64 times to get the raw data. The scanning step equals to 1 pixel, the spot size is 1 pixel, and the separation of each spot is 8 pixels. The pixel size of the projecting pattern is 174 nm and the simulated detection device has a pixel size of 87 nm, which is approximately the same as our experimental setup using a 63× object lens presented in the next section. The parameter k mentioned in Eq. (5) starts at 1 in our simulation, and $k_{\text{update}} = k/2$ when the function value f becomes greater than the former value. The objective lens (OL) has a NA of 0.5 and a total magnification power 63×. Both the excitation wavelength and the detection wavelength are assumed to be 680 nm in our simulations.

As shown in Figs. 1(b)–1(d), all reconstructed results of piFP, PE-SIMS-PR, and PEFP greatly improve the resolution compared with the filtered wide-field result (a). The 2× resolution enhancement result is shown in the upper left of Fig. 1(e). The resolution improvement of piFP achieves 1.84×, and PE-SIMS-PR achieves 1.59× under the Rayleigh criterion compared with the deconvolved wide-field result. PEFP performs better than PE-SIMS-PR with a 1.79× resolution enhancement, which can be proved by the normalized intensity profile shown in Fig. 1(f). But we can see that PEFP may bring more artifacts than both piFP and PE-SIMS-PR.

The performance of piFP reduced a great deal when 18% shift errors were introduced in our simulations [Fig. 2(b), upper right]. The shift errors bring distortions to the reconstruct result of piFP and reduce the resolution enhancement of piFP, while PEFP and PE-SIMS-PR remain almost the same.

PEFP also shows high reliability against noise, which is illustrated in Fig. 3. While 30% Gaussian noise will reduce the SNR and resolution of the output reconstructed image, PEFP works fine when 20% Gaussian noise is introduced into the raw data. It may be worthwhile to point out that 64 images are applied in our simulation. If more images with the same SNR are acquired, the reconstructed result will become better than that showed in Fig. 3.

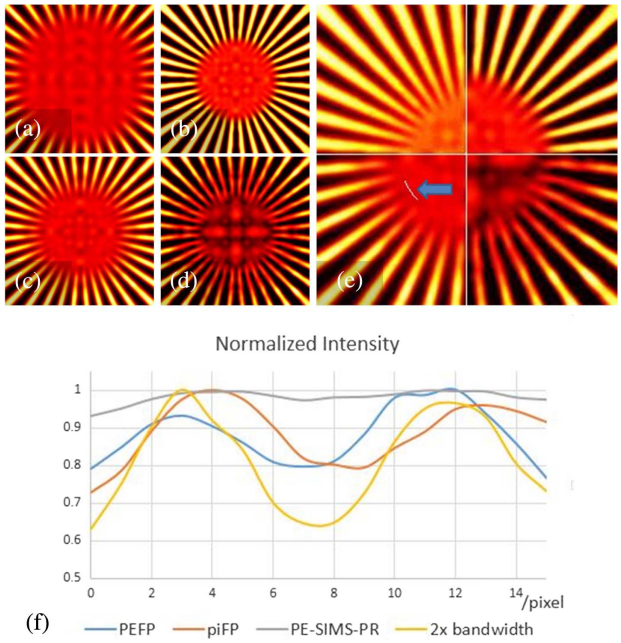

Fig. 1. Simulation of the standard object: (a) deconvolved wide-field image; (b) reconstructed image of piFP; (c) reconstructed image of PE-SIMS-PR [11]; and (d) reconstructed image of PEFP. The collage of the reconstructed image is shown in (e). Upper left, 2× bandwidth (NA = 0.5 × 2 = 1) filtered image; upper right, piFP; lower right, PEFP; and lower left, PE-SIMS-PR. (f) Normalized intensity profile along the curve indicated by the blue arrow.

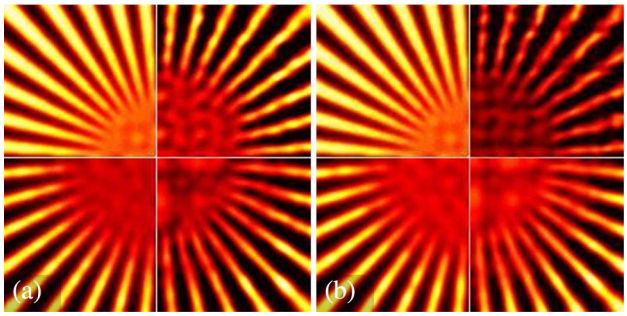

Fig. 2. Simulation result when (a) 9% and (b) 18% shift errors were introduced in the simulation. Upper left, 2× bandwidth filtered result; upper right piFP; lower right, PEFP; and lower left, PE-SIMS-PR.

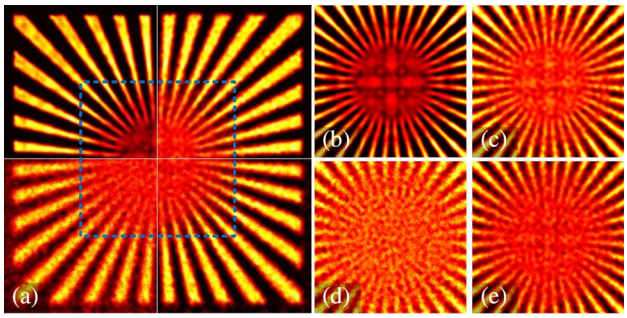

Fig. 3. (a) PEFP reconstructed image with different Gaussian noise; upper left, PEFP recovery image without noise; upper right, 10% Gaussian noise; lower right, 20% Gaussian noise; and lower left, 30% Gaussian noise. (b)–(e) are the reconstruct results within the dashed blue square shown in (a).

As a digital aberration correction step [Eq. (11)] is introduced, PEFP shows high resistance towards different types of aberrations, as shown in the simulation result in Fig. 4. Although aberrations will make the reconstructed result without digital aberration correction much poorer than that in Fig. 3(b), the reconstructed results in Figs. 4(g)–4(i) are similar to the reconstruction result in Fig. 3(b), where aberrations do not exist.

4. SYSTEM SETUP

The system setup that is used in our experiment is shown in Fig. 5.

A laser (Coherent, OBIS 647LX, 120 mW) is used in our experiment. Through a reflector, a collimating lens (AC254-100-A-ML, $f = 100$ mm), and the second reflector, the expanded laser beam is introduced to a digital mirror device (DMD; 1.143 cm, 854 × 600 pixels, pixel size 11 μm). A dichroic mirror (Chroma, TRF89902-ET-405/488/561/647 nm) and a filter (Chroma, ET690/50 m, 25 mmR) block the reflected illumination light. The sample images are taken with a charge-coupled device (CCD; DVC-1500M-T1, 1392 × 1040 pixels, pixel size 6.45 μm) through an object lens (63× PL Fluotar 63×/0.7, Leica for beads and Nikon, Apo TIRF, 100×/1.49 oil for the microtubule), a reflector, a dichroic mirror, a filter, and a 200 mm convex tube lens.

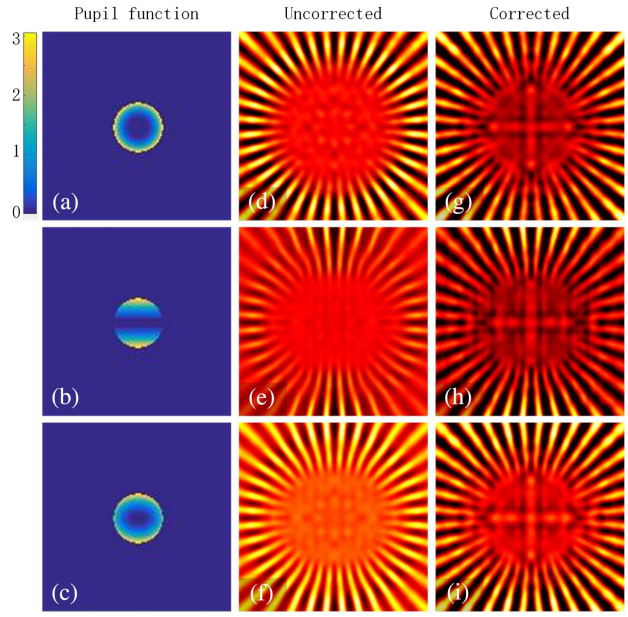

Fig. 4. (a) Pupil function under spherical aberration and (b) under astigmatism. The pupil function with spherical aberration, astigmatism, and defocus is shown in (c). (d)–(f) are the reconstructed results without a digital aberration correction step, and (g)–(i) are the corrected results. The maximum phase difference is around 3, represented by the yellow region in (a)–(c).

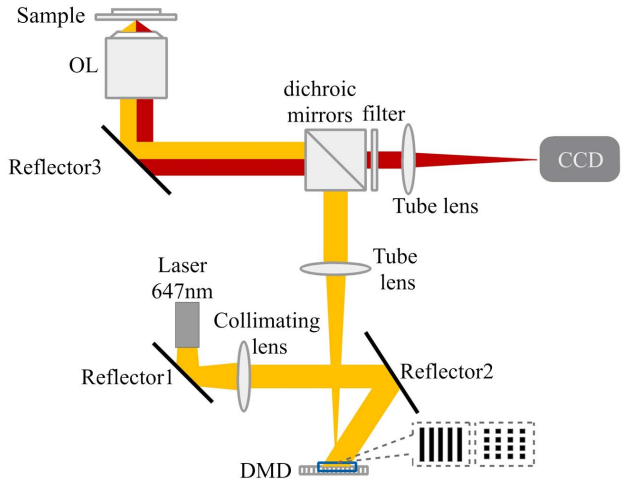

Fig. 5. System setup in our experiment. Typically, a DMD is applied to generate different illumination patterns, such as a sinusoidal pattern, a random speckle, or the multispot pattern that is applied in this work.

5. EXPERIMENTAL RESULTS

In Fig. 6, we generate a multispot illumination pattern, which is projected onto the object with demagnification of 63×, and shift the pattern 36 times (6 times in the x direction and 6 times in the y direction after each shift in the x direction) with a scanning step that is approximately the same size of the FWHM of the detection PSF. The multispot illumination pattern we use is slightly different from others, as additional shifts in

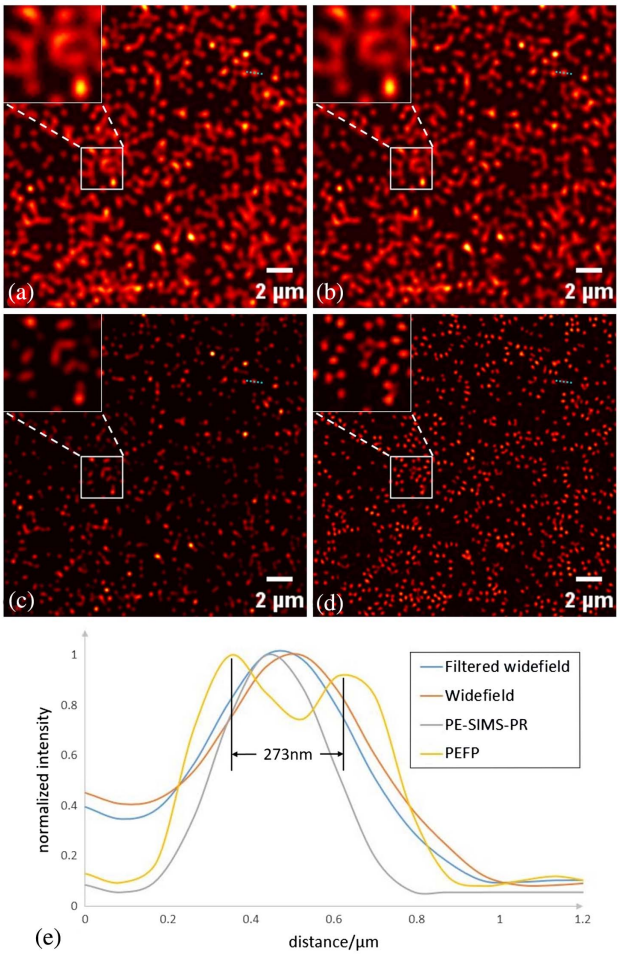

Fig. 6. Experimental results using fluorescent beads: (a) wide-field image; (b) a filtered wide-field image; (c) reconstructed image using PE-SIMS-PR algorithm; (d) reconstructed result using PEFP; and (e) normalized intensity profile of the cyan line shown in (a)–(d). Nominal bead diameter: 200 nm.

the y direction are applied each time we shift our pattern in the x direction. Here we set the additional shift to 1 pixel on the DMD that generates the illumination pattern. The multispot pattern used in this experiment has a separation length of 18 pixels between two spots, and each square spot has a length of 6 pixels on the DMD.

Dark red fluorescent beads (excitation wavelength: 660 nm/emission wavelength: 680 nm) with mean diameter of 200 nm (F8807, ThermoFisher) are imaged in our experiment. We have applied four iterations described in Section 2.B.3 in our algorithm, and in each iteration the reconstruction algorithm runs about 30 times to obtain the results in Fig. 6. As shown in Figs. 6(c)–6(e), PEFP provides a much better result than the reconstructed image using PE-SIMS-PR as the aberrations are corrected. Moreover, the reconstructed intensity distribution of the beads has been changed by the algorithm proposed in Ref. [11], while PEFP does not change the intensity distribution of the whole sample after the reconstruction. PEFP can distinguish two beads separated by 273 nm, as shown in Fig. 6(e), which is approximately 1.78× resolution enhancement compared with a wide-field image.

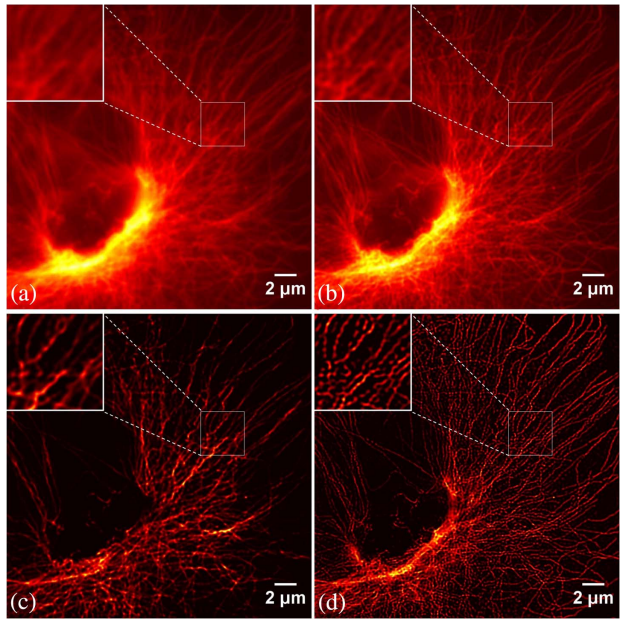

Fig. 7. Image of microtubule: (a) wide-field result; (b) filtered wide-field; (c) reconstruct image of PE-SIMS-PR; and (d) result image using PEFP.

We have also verified our method using a microtubule that is labeled by Abberior STAR 635P (excitation wavelength: 638 nm/emission wavelength: 651 nm). The object lens used in this experiment is Nikon, Apo TIRF, 100×/1.49 oil. A total number of 36 illumination patterns generated on the DMD with a demagnification 100× are projected onto the sample. The multispot pattern has a scanning step equal to 220 nm with a spot size equal to 440 nm and a separation of 1.32 μm on the sample plane.

As shown in Figs. 7(c) and 7(d), PEFP provides a better resolution enhancement as well, and we can see that information seems to be lost in Fig. 7(c) again due to low signal power, as we mentioned earlier.

6. CONCLUSION

As most algorithms based on iteration do, PEFP runs about twice the time that it takes using a noniterative algorithm in general. It may be worthwhile to point out that a high-background fluorescent signal will bring artifacts into our algorithm, as shown in Fig. 6(d). However, the method that we proposed provides the possibility of extending the application of pattern-illuminated FP microscopy, as it does not require prior knowledge of the scanning step of each illumination pattern. We have validated PEFP using both standard fluorescent beads and a fixed microtubule. Both the simulation and experimental results show that PEFP produces a high-resolution image that is insensitive to shift error or rotational error of the illumination patterns. As we reconstruct the illumination patterns separately, random speckle patterns that are demonstrated in Ref. [9] would also work in PEFP, which could extend PEFP to random speckle illumination patterns. In addition, we also

demonstrate a better resolution improvement than the existing PE-SIMS-PR method, which is better than blind-SIM [11].

Funding. National Key Research and Development Program of China (2016YFF0101400); National Basic Research Program of China (2015CB352003); National Natural Science Foundation of China (NSFC) (61335003, 61377013, 61378051, 61427818); Natural Science Foundation of Zhejiang Province (LR16F050001); Fundamental Research Funds for the Central Universities (2017FZA5004).

[†]These authors contributed equally to this work.

REFERENCES

1. S. W. Hell and J. Wichmann, "Breaking the diffraction resolution limit by stimulated emission: stimulated-emission-depletion fluorescence microscopy," Opt. Lett. **19**, 780–782 (1994).
2. E. Betzig, G. H. Patterson, R. Sougrat, O. W. Lindwasser, S. Olenych, J. S. Bonifacino, M. W. Davidson, J. Lippincott-Schwartz, and H. F. Hess, "Imaging intracellular fluorescent proteins at nanometer resolution," Science **313**, 1642–1645 (2006).
3. M. J. Rust, M. Bates, and X. Zhuang, "Sub-diffraction-limit imaging by stochastic optical reconstruction microscopy (STORM)," Nat. Methods **3**, 793–796 (2006).
4. M. G. Gustafsson, "Surpassing the lateral resolution limit by a factor of two using structured illumination microscopy," J. Microsc. **198**, 82–87 (2000).
5. R. Heintzmann and C. G. Cremer, "Laterally modulated excitation microscopy: improvement of resolution by using a diffraction grating," Proc. SPIE **3568**, 185–196 (1999).
6. S. A. Shroff, J. R. Fienup, and D. R. Williams, "Phase-shift estimation in sinusoidally illuminated images for lateral superresolution," J. Opt. Soc. Am. A **26**, 413–424 (2009).
7. K. Wicker, "Non-iterative determination of pattern phase in structured illumination microscopy using auto-correlations in Fourier space," Opt. Express **21**, 24692–24701 (2013).
8. K. Wicker, O. Mandula, G. Best, R. Fiolka, and R. Heintzmann, "Phase optimisation for structured illumination microscopy," Opt. Express **21**, 2032–2049 (2013).
9. E. Mudry, K. Belkebir, J. Girard, J. Savatier, E. L. Moal, C. Nicoletti, M. Allain, and A. Sentenac, "Structured illumination microscopy using unknown speckle patterns," Nat. Photonics **6**, 312–315 (2012).
10. J. Min, J. Jang, D. Keum, S. W. Ryu, C. Choi, K. H. Jeong, and J. C. Ye, "Fluorescent microscopy beyond diffraction limits using speckle illumination and joint support recovery," Sci. Rep. **3**, 2075 (2013).
11. L. H. Yeh, L. Tian, and L. Waller, "Structured illumination microscopy with unknown patterns and a statistical prior," Biomed. Opt. Express **8**, 695–711 (2017).
12. A. G. York, S. H. Parekh, N. D. Dalle, R. S. Fischer, K. Temprine, M. Mione, A. B. Chitnis, C. A. Combs, and H. Shroff, "Resolution doubling in live, multicellular organisms via multifocal structured illumination microscopy," Nat. Methods **9**, 749–754 (2012).
13. S. Dong, P. Nanda, R. Shiradkar, K. Guo, and G. Zheng, "High-resolution fluorescence imaging via pattern-illuminated Fourier ptychography," Opt. Express **22**, 20856–20870 (2014).
14. S. Dong, P. Nanda, K. Guo, J. Liao, and G. Zheng, "Incoherent Fourier ptychographic photography using structured light," Photon. Res. **3**, 19–23 (2015).
15. G. Zheng, R. Horstmeyer, and C. Yang, "Wide-field, high-resolution Fourier ptychographic microscopy," Nat. Photonics **7**, 739–745 (2013).
16. C. Kuang, Y. Ma, R. Zhou, G. Zheng, Y. Fang, Y. Xu, X. Liu, and P. T. So, "Virtual k-space modulation optical microscopy," Phys. Rev. Lett. **117**, 028102 (2016).
17. X. Ou, G. Zheng, and C. Yang, "Embedded pupil function recovery for Fourier ptychographic microscopy," Opt. Express **22**, 4960–4972 (2014).